Atomistic simulations of solid-phase epitaxial growth in silicon

Noam Bernstein* and Michael J. Aziz
Division of Engineering and Applied Sciences, Harvard University, Cambridge, Massachusetts 02138

Efthimios Kaxiras
Division of Engineering and Applied Sciences, Harvard University, Cambridge, Massachusetts 02138
and Physics Department, Harvard University, Cambridge, Massachusetts 02138
(Received 19 October 1999)

High-quality semiconductor crystals can be produced by solid-phase epitaxial growth at the amorphous-crystal interface. Despite extensive experimental studies, the microscopic mechanisms that lead to crystallization are not known. Molecular-dynamics simulations of a Si(001) amorphous-crystal interface, using an accurate empirical interatomic potential, give an activation energy (for $T > 950\,\mathrm{K}$) and a shape for the activated state that are in reasonable agreement with experimental measurements. Analysis of the simulations reveals complex microscopic mechanisms involving one or several consecutive atomic rearrangement steps; the unanticipated level of complexity casts doubt on the common viewpoint of a unique mechanism.

Epitaxial crystal growth from the vapor or melt has attracted much attention in recent years, motivated both by a fundamental interest in understanding growth phenomena and by the practical goal of controlling and improving growth of technologically important materials. Epitaxy can also occur at the amorphous-crystal interface, when the metastable amorphous phase is consumed upon heating to produce the stable crystalline phase. This process, called solid-phase epitaxial growth (SPEG), is the subject of intense research efforts aimed at producing high quality semiconductor thin films. Like the vapor-crystal and melt-crystal interfaces, the amorphous-crystal interface separates a disordered, uniform phase from a highly ordered phase. Unlike growth from the vapor or melt, however, in SPEG the mobility of atoms is everywhere so low that the rate limiting step is their rearrangement at the interface, rather than long-range thermal or atomic transport. It is therefore of great interest to investigate the possible microscopic mechanisms for SPEG, where the dynamics of atoms at the growth front could be very different from the usual growth situations. Moreover, since this process occurs in the middle of a bulk sample, surface experimental probes with atomic resolution are ineffective. Instead, experiments have been confined to measuring macroscopic, average quantities such as the activation energy, activation strain, and the dependence on substrate orientation and doping, all of which have direct bearing on models for the atomistic processes.[1,2]

In this work we present the results of extensive molecular-dynamics (MD) simulations of the amorphous-crystal interface in Si(001) with the aim of developing a microscopic understanding of SPEG mechanisms, an issue that has not been addressed in earlier simulations.[3] We study samples at different external temperatures and applied pressures, including several different stress states, in order to measure key thermodynamic parameters such as the activation energy and diagonal components of the strain tensor. By monitoring the paths of atoms in a sequence of configurations generated by MD as they evolve from amorphous to crystal we identify examples of microscopic mechanisms for growth at the interface. These demonstrate a heretofore unanticipated level of complexity in this process at the microscopic scale, casting some doubt on the common viewpoint of a unique SPEG mechanism.

In experiment, the position of the interface can be measured using the interference between laser beams reflected by the sample-vacuum and the amorphous-crystal interfaces.[1] The derivative of this position as a function of time is the interface speed, which is time independent and exhibits Arrhenius behavior with temperature T and stress σ_{ij}:

$$v(T) = v_0 \exp[-(E^* - \sigma_{ij} V^*_{ij})/k_B T], \tag{1}$$

where v_0 is an orientation-dependent velocity prefactor, E^* is the activation energy, and V^*_{ij} is the activation strain tensor.[4] The activation volume is given by $V^* = \mathrm{Tr}[V^*_{ij}]$. At zero stress, this relation describes accurately the interface speed as a function of temperature over a range of 800 K, spanning five decades in v, with $E^* = 2.68 \pm 0.05\,\mathrm{eV}$ (Ref. 1) ($E^* = 2.75 \pm 0.05\,\mathrm{eV}$, and v spans ten decades for As-doped samples[1]). The temperature-independent activation energy is suggestive of a unique microscopic mechanism that controls growth. Hydrostatic pressure experiments reveal an activation volume $V^* = -0.28\,\Omega_{\mathrm{Si}}$, where Ω_{Si} is the atomic volume of Si in its bulk diamond phase (at standard temperature and pressure). By applying nonhydrostatic stress the elements of the activation strain tensor V^*_{ij} can be measured. It is harder to study the nonhydrostatic stress effects quantitatively, but it is clear that the activated state is shortened along z and elongated along xy,[4–6] i.e., $V^*_{zz} < 0$ and $V^*_{xx} + V^*_{yy} > 0$, where the growth direction z is perpendicular to the (001) interface.

Simulations of SPEG require the evolution of samples large enough ($\sim 10^3$ atoms) to realistically capture the features of both phases and the interface for millions of MD time steps. Simulations of this scope are at present feasible only through the use of empirical interatomic potentials. The main concern in using such potentials is their reliability in accurately reproducing quantities to which they were not fit.

 ©2000 The American Physical Society

In our studies we have used a recently developed interatomic potential for silicon, referred to as the environment dependent interatomic potential[7] (EDIP). This potential gives a very good description of diamond structure silicon, including point defects and activated bulk diffusion processes, by virtue of having been fit to such structures. It has also proven very reliable in reproducing the structure of amorphous silicon, to which it had not been fit. We are therefore confident that the EDIP potential provides as reasonable a description of SPEG as any existing model potential for silicon.

In our MD simulations we use the Gear predictor-corrector algorithm to evolve the system in time, and rescale the atomic velocities to keep the temperature constant. We use an extended system Parrinello-Rahman approach[8] to maintain constant stress. We create the amorphous phase by simulating the quenching of a liquid silicon sample. After annealing a quenched sample at 1000 K for several million time steps, we obtain a fourfold coordinated continuous random network structure with a coordination defect density less than 5%. By joining one such amorphous sample consisting of about 1200 atoms to a bulk crystal sample consisting of about 800 atoms we create a sample with two interfaces between the two phases, due to the periodic boundary conditions. Extensive annealing at 1000 K allows the interface to relax to a reasonable structure of low energy. The resulting interface structure is similar to what we reported earlier based on tight-binding calculations.[9] In the course of an MD simulation, images of the sample viewed parallel to the interface along (100) directions of the crystal clearly indicate that the crystalline portion increases until the entire sample has crystallized with a few remaining point defects. We make sure that this process corresponds to SPEG rather than growth from the melt by monitoring the average coordination of atoms throughout the sample, which would undergo a discontinuous change if the amorphous phase were to melt; such a change is not observed in our simulations.

First we attempt to make contact to the thermodynamic experimental measurements of SPEG, i.e., the activation energy and strain tensor, using the results of our simulations. To determine the growth rate of the crystal during a long MD simulation we plot the number of ''crystal atoms'' vs time, and fit to a line. The number of ''crystal atoms'' must be determined automatically during the simulation, which requires the instantaneous and unambiguous identification of ''crystalline'' versus ''amorphous'' atoms. To this end we compute χ, the sum of the absolute values of the dot products between bond directions around each atom and the bond directions in the underlying crystal lattice which is a continuation of the substrate. This quantity is quite sensitive to orientational order, and therefore to the difference between the two phases. $\chi=4$ in the perfect crystal, whereas it averages 2.7 in the amorphous phase.[10] We define a criterion for crystallinity that includes both a threshold in the value of χ (3.3), and the requirement that the crystalline part of the sample be contiguous. In Fig. 1(a) we plot the interface speed vs inverse temperature. At each temperature we ran several simulations by restarting with random atomic velocities. The chaotic character of the system causes the different MD runs to diverge quickly, and to lead ultimately to different samples of the same (T, σ_{ij}) ensemble. Since it appears that the slope

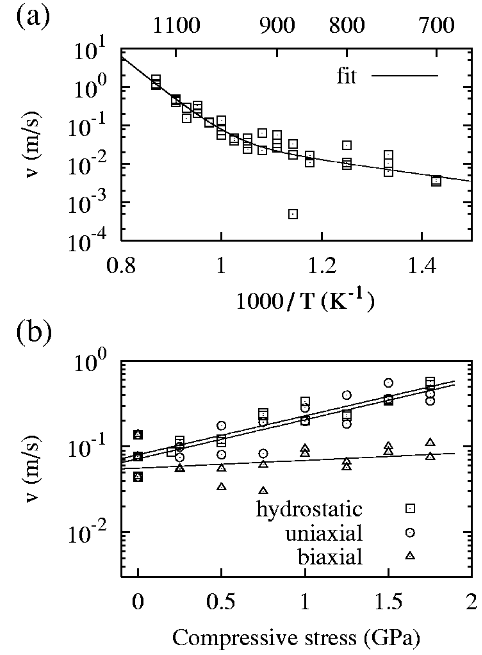

FIG. 1. Arrhenius fits for the growth rate v versus: (a) $1/T$, fitted to a sum of two activated processes with different activation energies; (b) the diagonal components of the strain tensor V^*_{ii}.

is different at low and high temperatures, we fit the data to the sum of two Arrhenius terms with different prefactors and activation energies.

At low temperature ($T<950$ K) a mechanism with an activation energy of 0.4 ± 0.2 eV dominates, while at higher temperatures the dominant mechanism has an activation energy of 2.0 ± 0.5 eV. The experimental results[1] exhibit just one activation energy, 2.7 eV,[5] which has been interpreted as corresponding to a defect-formation energy of 2.3 eV and a defect-migration energy of 0.4 eV.[2] The existence of two different activation energies in the simulation is consistent with the extrinsic presence of defects that are responsible for growth. At low temperatures existing defects (which are quenched in during the preparation of the sample) dominate and the activation energy is just the migration barrier for these defects (in agreement with the experimental interpretation). At high temperature new defects are created thermally and the activation energy is the sum of the formation and migration energies. This is consistent with the fact that simulations, due to the extremely high quenching rates, generally have higher defect (miscoordinated atom) densities than experiment: defect densities are a few percent in our samples, whereas experimental values range from 0.01% to 1%.[12] Our explanation is also consistent with the observation of a much lower activation energy in experiments where large numbers of defects are generated athermally, for example during ion-beam enhanced SPEG.[13]

An additional thermodynamic measurement is the activation volume and its shape, determined by pressure and stress experiments. To probe the shape of the activated state we apply nonhydrostatic stress to the sample during SPEG. By applying uniaxial compression perpendicular to the interface (varying σ_{zz}) and biaxial compression parallel to the interface (varying σ_{xx} and σ_{yy}), we extract the corresponding elements of the activation strain tensor V^*_{zz} and $V^*_{xx}+V^*_{yy}$.

TABLE I. Activation energy E^* and migration component E^m, activation volume V^*, and diagonal strain tensor elements V^*_{ii}. (a) Experiment: E^* from Ref. 1, E^m from Ref. 2, V^* from Ref. 2, $V^*_{xx}+V^*_{yy}$ from Ref. 4, and V^*_{zz} from Refs. 5 and 6. (b) Fit of simulation results to Arrhenius behavior. (c) Analysis of atomistic mechanisms (these values may not be unambiguously assigned to activation or migration, see text for discussion). Energies in eV, volumes in units of Ω_{Si}.

	E^*	E^m	V^*	$V^*_{xx}+V^*_{yy}$	V^*_{zz}
(a) Experiment	2.7 ± 0.05	0.4	-0.28 ± 0.03	$+0.30\pm0.01$	-0.35 ± 0.04
(b) Simulation	2.0 ± 0.5	0.4 ± 0.2	-0.71 ± 0.10	-0.08 ± 0.12	-0.74 ± 0.15
(c) Atomistics	[0.2,1.4]		[−0.1,0.0]	[−0.6,+0.2]	[−0.1,+0.1]

Results of annealing runs at a range of stresses in hydrostatic, uniaxial, and biaxial geometries are plotted in Fig. 1(b). Fitting these results to an Arrhenius form gives the activation strain tensor (Table I). Within the margins of error (determined by the scatter in the results), the calculated activation strain tensor elements satisfy the consistency relation $V^*=\mathrm{Tr}[V^*_{ij}]$.[4] In contrast, the experimental measurements (also listed in Table I), do not satisfy the consistency relation, a fact ascribed to a number of experimental difficulties.[5,6] There is qualitative agreement between our simulations and experiment: in both cases V^*_{zz} is large and negative, and almost equal to V^*, whereas $V^*_{xx}+V^*_{yy}$ is either smaller or possibly of the opposite sign (the lack of consistency in the experimental results precludes a more definitive assignment). This qualitative agreement is quite a subtle test of the accuracy of the simulation.

Given the inability of experiment to probe the microscopic features of SPEG, one of the important contributions of the simulation is to identify possible microscopic mechanisms for the crystallization process. To this end, we first need to define what is meant by a ''microscopic mechanism.'' Because the structure of the amorphous phase is well represented by a continuous random network, we expect a mechanism to consist of an ordered sequence of local connectivity changes. To identify mechanisms in our simulation we begin with a sequence of configurations from an MD run, each one averaged over a few hundred time steps in order to smooth out thermal vibration. We then relax each configuration completely, and find network connectivity changes, i.e., atoms whose neighbor lists have changed between consecutive time steps. These ''active atoms'' are partitioned into clusters, each including active atoms that are nearest neighbors or share a nearest neighbor. Clusters in consecutive time steps that share some active atoms are grouped together into mechanisms. Defined in this way, each mechanism specifies an ordered progression of localized network rearrangements. Since the system is large and many unrelated changes occur simultaneously in different parts of the unit cell, it is necessary to consider the energetics of each mechanism independently from all others. Simply computing the energy barrier for transformation from one configuration to the next could potentially superpose energy changes from several unrelated mechanisms. To freeze out unrelated motion while studying the energetics of a particular mechanism we produce a series of composite configurations: the positions of atoms in the mechanism and their nearest neighbors are taken from the relaxed MD configurations, while all other atoms are fixed at the positions they had at the initial configuration of the mechanism. Uniform strain fluctuations, introduced by the composite configuration into the MD configuration, must be prevented from causing translation of active atoms with respect to the rest of the system. To achieve this, we deform all configurations to the initial unit-cell size and shape. The composite configurations thus produced are again fully relaxed, including both the unit-cell size and shape and the atomic positions.

To find the pathways in configuration space that connect the initial and final configurations in each mechanism we use a simple version of the elastic band method for studying chemical reactions:[11] we define a chain of configurations in configuration space connecting initial and final configurations in the mechanism; the total energy of this chain is the sum of the energies of each configuration plus a harmonic potential in the distance between each pair of configurations along the chain that are farther than some cutoff distance. This energy is minimized with respect to all the atomic positions in every configuration in the chain. Then the unit-cell size and shape of each configuration is relaxed independently, and the process is repeated until convergence. We attempted to extract mechanisms from several segments of the MD runs, but here we will discuss examples from a 5×10^5 fs segment of a 1025 K, zero stress MD run. During this period 16 atoms appeared to crystallize. These atoms were divided into seven clusters, including one cluster of six adjacent atoms. We were able to identify mechanisms during which crystallization occurred for every case except the largest cluster, where the motion was too complicated to follow.

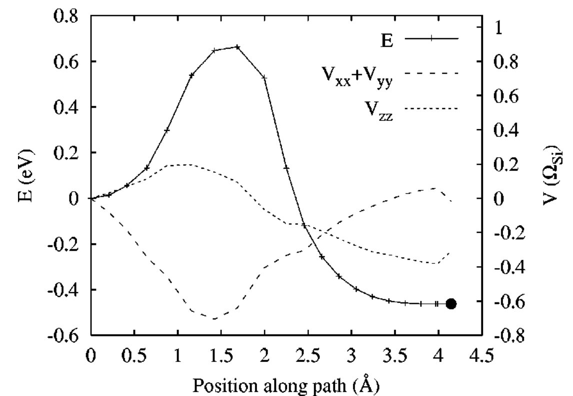

FIG. 2. Energy along a crystallization path for a simple mechanism. Points marked by black dots are relaxed configurations taken from time-averaged snapshots, with atomic motion outside the active region frozen out. The line is a low-energy path connecting these configurations, relaxing atoms along the path. Diagonal components of the activated strain tensor are also shown by broken lines (see text for details).

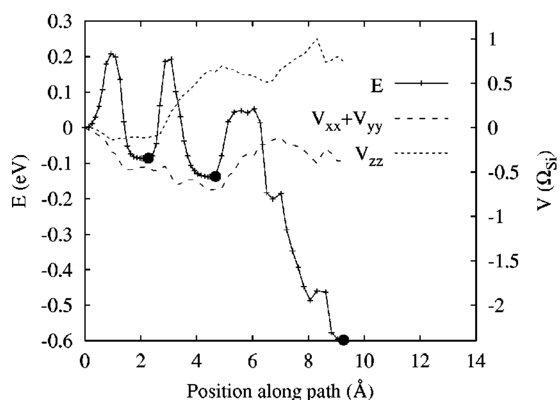

FIG. 3. Energy along a crystallization path for a complex mechanism. Notation is the same as for Fig. 2.

The transformation paths can be classified into two types: simple events involving only one step, and complex ones involving the creation and annihilation of metastable defects. The energies and diagonal components of the strain tensor along the transformation path for one simple mechanism and one complex mechanism are shown in Figs. 2 and 3. The simple mechanism reduces the energy of the system by 0.45 eV, with an energy barrier of 0.66 eV. Of the complex events, only one leads to a lowering of the energy, by 0.6 eV, with a barrier of 0.2 eV. The strains at the peak energy configuration for the different mechanisms are widely scattered (see Table I).

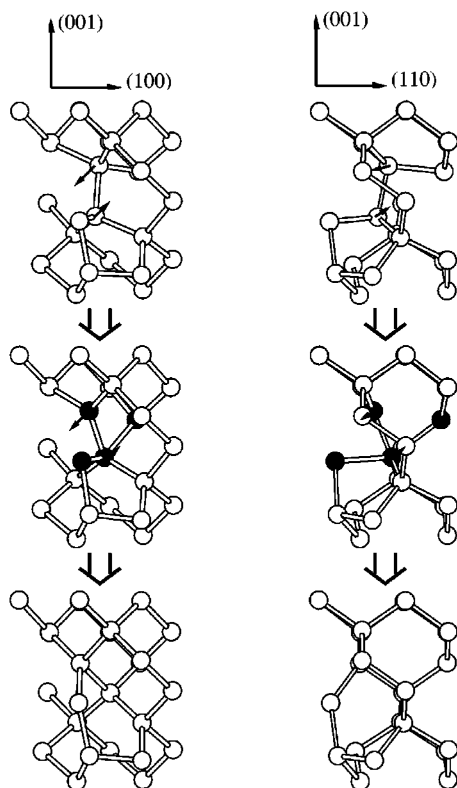

FIG. 4. Illustration of a simple mechanism for crystallization. The initial (top), saddle-point (middle), and final (bottom) configurations are shown. Two different views of the interface along high-symmetry directions of the crystal are shown for each step; the crystalline part is in the upper half of each figure. In this example two atoms perform a partial rotation, indicated by the small arrows, and end up in crystalline positions. Undercoordination defects, indicated by the black atoms, exist only at the saddle-point configuration.

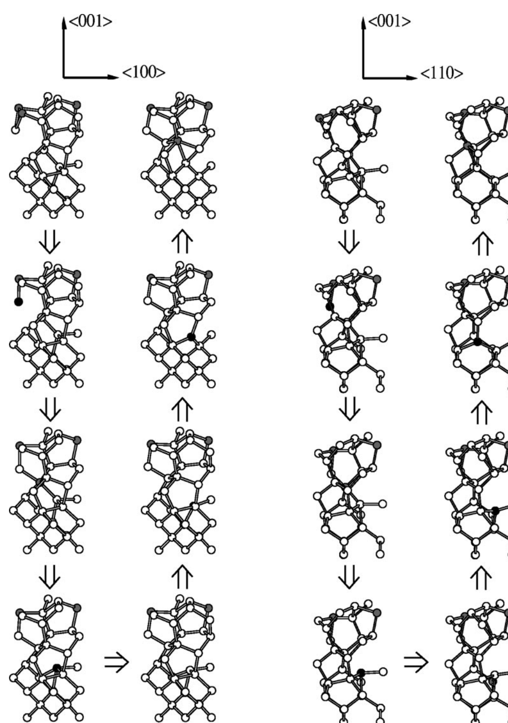

FIG. 5. Illustration of a complex mechanism for crystallization. The sequence of steps starts at the upper left and proceeds down the left column, then continues at the bottom right and proceeds up the right column, as indicated by the double arrows. Two views are shown for every step, along high-symmetry directions of the crystalline part, which is in the lower half of each image. Comparison between the initial (top left) and final (top right) steps makes clear the changes in the bonding at the interface due to crystallization of two atoms. Configurations are shown that correspond to each major local maximum and minimum of the energy in Fig. 3, as well as a configuration half way between the last local maximum and the final configuration. Atoms with coordination other than 4 are shown shaded: black for threefold coordination, gray for fivefold coordination. During this mechanism, a fivefold coordination defect migrates to the interface in the first six steps; this facilitates the crystallization of two atoms, which takes place in the last two steps.

The atomistic mechanisms always include the migration part of the crystallization mechanism; the formation part is included only if it occurs sufficiently closely in time to the migration. In contrast, both experiment and the Arrhenius fits of high-temperature MD runs involve the migration and formation of defects. This makes direct comparison between the microscopic and macroscopic measurements difficult. In the instances where the microscopic mechanism only captures the migration of the defect, the remainder of the full crystallization mechanism (i.e., defect formation) is likely to occur in some region of the system separated in space or time from the crystallization event. It would be extremely difficult to make such connections in an unambiguous way with current MD capabilities.

To illustrate these points we present the atomic structure of the simple and complex mechanisms whose energetics are discussed above in relation to Figs. 2 and 3. In Fig. 4 we

show three different atomic configurations corresponding to a crystallization event by the simple mechanism (see Fig. 2). The initial, saddle-point and final configurations are shown. Through this sequence of steps two atoms crystallize by undergoing a process reminiscent of the concerted exchange mechanism,[14] by which atoms can interchange positions in bulk Si. In the initial and final configurations all atoms in the neighborhood of the two exchanging atoms are fourfold coordinated, while in the saddle-point configuration several coordination defects have been formed (the two exchanging atoms and two of their neighbors are threefold coordinated). Thus in this example coordination defects are locally created and then annihilated by the crystallization process. The low energy of this mechanism (compared to the observed activation energy for growth) indicates that the local bonding in this configuration must be unusually weak, or such low energy mechanisms could dominate growth.

In Fig. 5 we show eight configurations along the multistep path of the complex mechanism, whose energy and strains were plotted in Fig. 3. In the first six configurations a coordination defect in the amorphous near the interface migrates in a series of steps, alternating between over coordination (fivefold) and under coordination (threefold). Once it is at the interface it facilitates the incorporation of two atoms into a sixfold ring at the edge of the crystal. This is consistent with the bimolecular defect flow mechanism in amorphous Si, postulated by Witvrouw and Spaepen,[15] in which a preexisting defect needs to be present to loosen up the network thereby making it possible for a flow event. It is clear from the images in Fig. 5 that the transformation begins with a preexisting defect whose nucleation is not included in the mechanism. Presumably the creation of this defect, operating in series with the observed migration, contributes the additional energy needed to explain the difference between the energy barrier of 0.2 eV obtained for this mechanism (see Fig. 3) and the activation energy of 2.0 eV for growth obtained from the thermodynamic analysis (see Fig. 1).

We have shown that an empirical potential simulation can reproduce the activation energy and strain for solid phase epitaxial growth, as well as provide a window into the microscopic rearrangements that occur during growth. In one class of mechanisms, probably relevant only where bonds are already weakened, crystallization occurs without the need for any preexisting defects. Another class of mechanisms involves the migration of pre-existing coordination defects, which can form long before they lead to crystallization. It is therefore difficult to add up the microscopic formation and migration contributions to the effective activation energy for growth. Until now this process had been modeled as a repeatable series of simple, thermally activated steps: coordination defects are created, migrate and are annihilated, facilitating the atomic rearrangements. The present simulations reveal that while this general framework is reasonable, the details of the process are in fact substantially more complex.

We thank F. Spaepen and W. Barvosa-Carter for many helpful discussions. This work was supported by the Harvard MRSEC which is funded by NSF Grant No. DMR-94-00396.

---

*Presently at the Center for Computational Materials Science, Naval Research Lab, Washington, DC.

[1] G. L. Olson and J. A. Roth, Mater. Sci. Rep. **3**, 1 (1988).

[2] G.-Q. Lu, E. Nygren, and M. J. Aziz, J. Appl. Phys. **70**, 5323 (1991).

[3] M.-J. Caturla, T. Diaz de la Rubia, and G. H. Gilmer, J. Appl. Phys. **77**, 3121 (1995).

[4] M. J. Aziz, P. C. Sabin, and G.-Q. Lu, Phys. Rev. B **44**, 9812 (1991).

[5] W. B. Carter and M. J. Aziz, in *Thin Films: Stresses and Mechanical Properties V*, edited by S. P. Baker, P. Børgesen, P. H. Townsend, C. A. Ross, and C. A. Volkert, MRS Symposia Proceedings No. 356 (Materials Research Society, Pittsburgh, 1995), p. 87.

[6] W. Barvosa-Carter, Ph.D. thesis, Harvard University, 1997.

[7] M. Z. Bazant, E. Kaxiras, and J. F. Justo, Phys. Rev. B **56**, 8542 (1997); J. F. Justo, M. Z. Bazant, E. Kaxiras, V. V. Bulatov, and S. Yip, *ibid.* **58**, 2539 (1998).

[8] M. Parrinello and A. Rahman, Phys. Rev. Lett. **45**, 1196 (1980); J. Appl. Phys. **52**, 7182 (1981); J. Chem. Phys. **76**, 2662 (1982).

[9] N. Bernstein, M. J. Aziz, and E. Kaxiras, Phys. Rev. B **58**, 4579 (1998).

[10] Our calculations for the same quantity in samples of bulk amorphous Si give a very similar value of 2.8.

[11] R. Elber and M. Karplus, Chem. Phys. Lett. **139**, 375 (1987).

[12] S. Roorda, W. C. Sinke, J. M. Poate, D. C. Jacobson, S. Dierker, B. S. Dennis, D. J. Eaglesham, F. Spaepen, and P. Fuoss, Phys. Rev. B **44**, 3702 (1991).

[13] F. Priolo and E. Rimini, Mater. Sci. Rep. **5**, 319 (1990).

[14] K. C. Pandey, Phys. Rev. Lett. **57**, 2287 (1986).

[15] A. Witvrouw and F. Spaepen, J. Appl. Phys. **74**, 7154 (1993).